Steel and Composite Structures, *Vol. 29*, *No. 1* (*2018*) *23-37*
DOI: https://doi.org/10.12989/scs.2018.29.1.023

Evaluation of seismic criteria of built-up special concentrically braced frames

Amin Izadi and Ali A. Aghakouchak *

Department of Civil and Environmental Engineering, *Tarbiat Modares University*, *Tehran*, *Iran*

(*Received January 13*, *2018*, *Revised July 18*, *2018*, *Accepted July 28*, *2018*)

Abstract. In this paper, seismic provisions related to built-up special concentrically braced frames (BSCBFs) are investigated under cyclic loading using non-linear finite element analysis of a single-bay single-story frame. These braces, which contain double angle and double channel brace sections, are considered in two types of single diagonal and X-braced frames. The results of this study show that current seismic provisions such as observing the 0.4 ratio for slenderness ratio of individual elements between stitch connectors are conservative in BSCBFs, and can be increased according to the type of braces. Furthermore, such increments will lead to decreasing or remaining the current middle protected zone requirements of each BSCBFs. Failure results of BSCBFs, which are related to the plastic equivalent strain growth of members and ductility capacity of the models, show that the behaviors of double channel back-to-back diagonal braces are more desirable than those of similar face-to-face ones. Also, for double angle diagonal braces, results show that the failure of back-to-back BSCBFs occurs faster in comparison with face-to-face similar braces. In X-braced frames, cyclic and failure behaviors of built-up face-to-face models are more desirable than similar back-to-back braces in general.

Keywords: build-up special concentrically braced frames; double angle; double channel; face-to-face; X-braced

1. Introduction

Steel concentric braced frames (CBFs) are frequently used as lateral load resisting systems in structural frames. CBFs can provide strength, stiffness, and ductility of structures due to their ability of deforming inelastically and enduring large cyclic demands of earthquake loadings. Based on AISC design codes (AISC 2010a and 2016), Special Concentrically Braced Frames (SCBFs), and Ordinary Concentrically Braced Frames (OCBFs) are two types of CBFs that should follow certain design rules. According to demands of design earthquake, OCBFs are expected to experience limited inelastic deformation in their members and connections, while SCBFs are expected to withstand significant inelastic deformation without considerable resistance reduction in their members and connections.

Capacity design methods require that plastic deformations must occur in braces; thus other frame members such as columns and beams must act elastically during earthquake. Several analytical and experimental studies such as (Jain and Goel 1978, Shaback and Brown 2003, Fell 2008, Lai *et al*. 2010, Hsu *et al*. 2011, D'Aniello *et al*. 2013) have been done to investigate inelastic behavior and energy dissipation of braces. In this regard, Tremblay (2002) has evaluated the experimental studies on phenomena such as buckling strength of braces, post-buckling behavior, maximum tensile strength, out-of-plane deformation, and fracture life of braces. His conclusions reveal that brace slenderness is the prevailing parameter affecting the seismic behavior of braces. Based on dissipated energy in braces of different section and slenderness, Lee and Bruneau (2005) demonstrate that compressive strength and energy dissipation capacity in compressive braces decrease dramatically for slenderness ratio over 80. In order to examine buckling and fracture behavior of different section shapes of braces, Fell *et al*. (2009) infer that width-to-thickness ratio is the most important parameter affecting the seismic behavior of brace members. Also, Tirca and Chen (2014) show that square HSS braces with larger slenderness ratios and lower width-to-thickness ratios have a longer fracture life. By testing the full scale X-braced specimens composed of double angle braces, Kanyilmaz (2017) demonstrates thatthe slenderness of compression members should be estimated withmore realistic boundary conditions.He also focuses on the stiffness and post-buckling influence of compression diagonal members on the global performance of concentric X-braced frames.

Quite a few experimental and analytical works have been done to enhance the ductile behavior of different geometric types of edge gusset plates, as one of the crucial factors influencing on the steel frame seismic behaviors. Published remarkable results such as (Astaneh-Asl *et al*. 1982, 1985, Astaneh-Asl 1998) show that, during the brace out of plane buckling, a linear clearance which corresponds to twice the thickness of edged-gusset plates (i.e., $2t_p$), can provide an appropriate condition for end rotation of the brace. In fact this conclusion is drawn from full scale tests on specimens made of double angle back to back braces that were subjected to cyclic loadings. In another study, in order to investigate different end rotation conditions of braces, some specimens composed of face-to-face and back-to-back

*Corresponding author, Professor,
E-mail: a_agha@modares.ac.ir

http://www.techno-press.org/?journal=scs&subpage=6

ISSN: 1229-9367 (Print), 1598-6233 (Online)

double angle braces have been tested. Test results of Aslani and Goel (1992) show that the more compression strength the built-up braces have, the less ductility such systems will exhibit and the earlier failure of the whole system will happen. Moreover, they concluded that cyclic dissipation energies in face-to-face section models are twice greater than the corresponding and similar back-to-back braces. The experimental results of Johnson (2005) show that as braces buckle under compression, formation of plastic hinges in the gusset is preferred to allow a ductile behavior of the frame. Also, the numerical results of Hadianfard and Khakzad (2016) confirm that besides of the influence of gusset plate size and thicknesses on the capacity, buckling, and post-buckling behavior of the brace frames, position of the bracing splice plate with respect to the free bending line is of great importance.

In this study, the effects of the provisions specified in AISC 341 on the seismic behavior of Built-up Special Concentric Braced Frames (BSCBFs) have been evaluated. In addition, in order to investigate the effects of built-up configuration on the cyclic behavior of such systems, both double channel and double angle BSCBFs have been employed in order to compare different cyclic and failure impacts of such configurations. For these purposes, a single bay single story frame, in the type of single diagonal and X-braced configurations and composed of different types of gusset plates, has been employed. The frames are modelled using nonlinear finite element methods (FEM), and their behavior under cyclic loading is simulated.

2. Verification and failure analysis

The basic model used in this study is a steel substructure based on experimental frames used in University of Washington (Fig. 1) (Johnson 2005 and Lehman *et al.* 2008). The height and width of the sub-assemblage are equal to 365 to 365 cm from member centerlines. This substructure includes a single diagonal brace (HSS12.7×12.7×0.95 cm), two beams (W17.8×40.9 cm), two columns (W30.4×31.2 cm), and two edge-gusset plates that connect the brace to beams and columns. An elliptical clearance at the end of the gusset plates equal to 6 times the thickness of connection member ($6t_p$) had been provided.

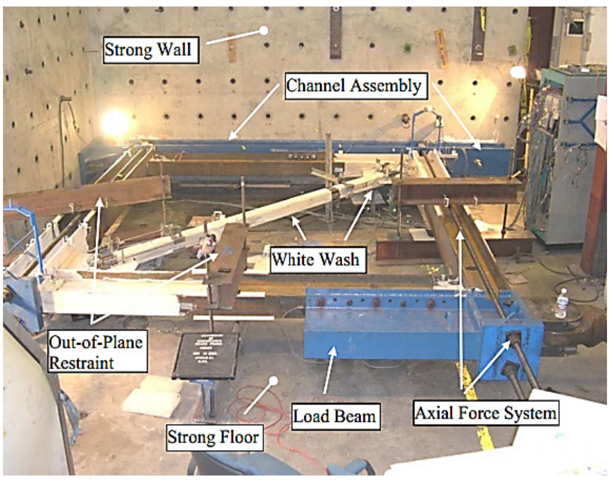

Fig. 1 UW specimens (adapted from Johnson 2005)

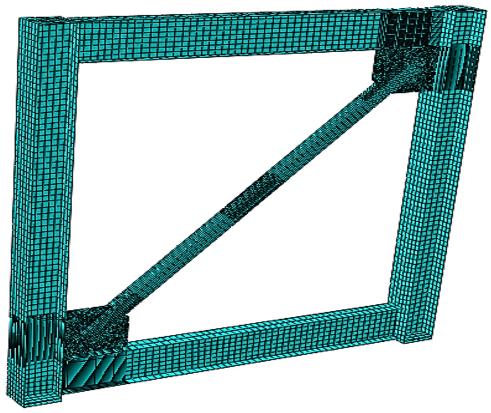

Fig. 2 FE verification model

Table 1 Steel properties of analysis models

	F_y (kgf/cm^2)	F_u (kgf/cm^2)	ε_u	E (kgf/cm)	υ
Beam	4119.6	5169.9	0.175	2038902.1	0.3
Column	3956.5	5261.7	0.217	2038902.1	0.3
Brace	4915.0	5322.9	0.082	2038902.1	0.3
Gusset plate	4629.5	5628.8	0.167	2038902.1	0.3

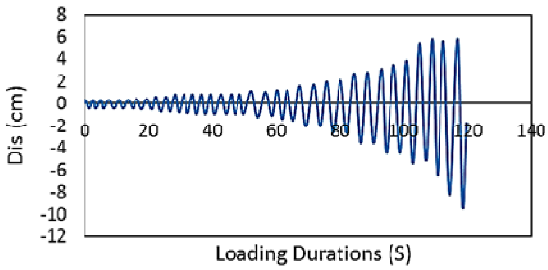

Fig. 3 Cyclic loading

Four node quadrilateral shell elements, which have six-degree-of-freedom in their nodes, have been used in the verification model (Fig. 2).The bottom of columns has been modeled as a pin and roller support. The flanges of beams and columns are restrained against out of plane buckling similar to the conditions of the experiment.

The cyclic lateral load, based on the experiment reports (Yoo 2006), have been applied to the beam of diagonal-braced sub-assemblage (Fig. 3). Table 1 shows the steel properties of braced frame used for verification of the results. Combined hardening material model are used to simulate cyclic inelastic behavior.

A relatively fine mesh (1 cm by 1 cm) is used in gusset plate connections and the whole length of the brace. Initial imperfection could play a significant role that affects the modes of failure and the shift in location of mid-length plastic hinge (Haddad 2015 and 2017). Based on the research done by Hassan *et al.* (2018), and in order to simulate out of plane buckling of the brace, an out of plane displacement is imposed as an initial imperfection, and the nonlinear-geometry combinations are employed in the model. For verifying the results of FE model, a detailed comparison between the analytical prediction and experimental observation has been made. In this regard, the analytical and experimental results of Yoo is shown in Fig. 4(a) (Yoo 2006).

FE cyclic force-displacement results of our model is also shown in Figs. 4(b) and (c). It can be observed that the FE model predicts the last tensile cycle strength with just 2.3% difference, compression strength with 1%, and the initial stiffness of frame with 0.7%. Therefore, the results of finite element analysis are very close to the experimental reports, and hence the numerical model is considered acceptable. As shown in Figs. 5(a) and (b), with regard to prediction of local buckling and stress distribution in the middle of the brace and gusset plates, FE verified model has created an acceptable simulation.

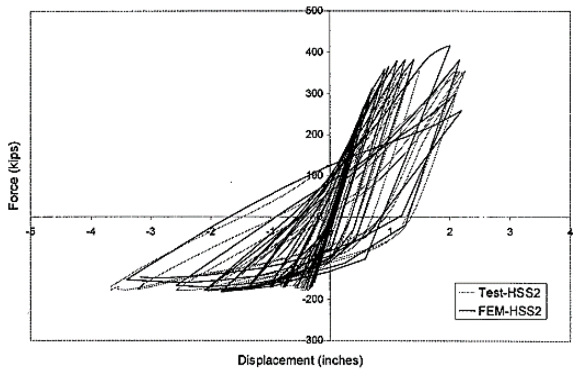

(a) Reference model- Test-HSS2 (Yoo 2006)

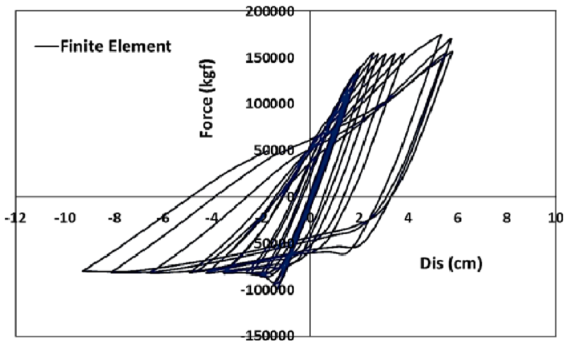

(b) FE verification result

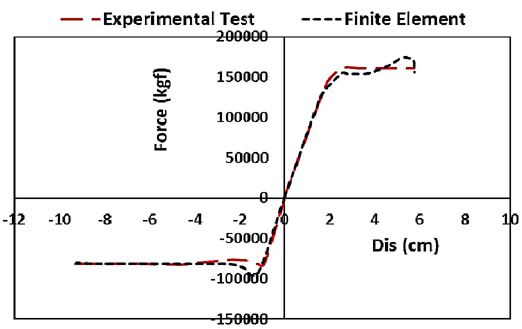

(c) Cyclic envelop curves

Fig. 4 Force-displacement cyclic curves (verification results)

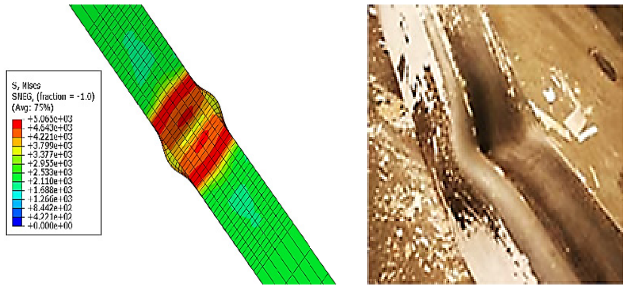

(a) Brace middle: FE analysis, experimental model

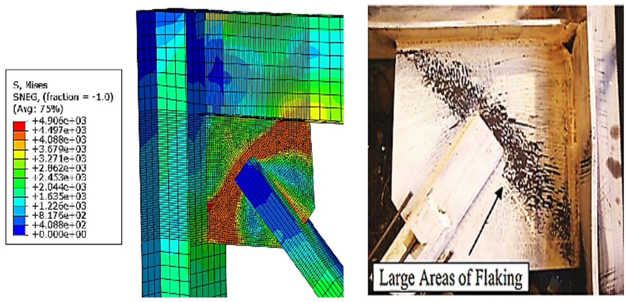

(b) Gusset plate: FE analysis, experimental model

Fig. 5 Von Mises Stress distribution of verification model

In this study, plastic equivalent strain index (ε_e^{-pl}) has been employed to investigate the local behavior of members, and predict common failure modes of BSCBFs in critical areas (Alipour and Aghakouchak 2013). In the Eq. (1), ε_0^{-pl} represents the primary plastic equivalent strain and ε^{pl} is the plastic strain.

$$\varepsilon_e^{-pl} = \varepsilon_0^{-pl} + \int_0^t \sqrt{\frac{2}{3}\dot{\varepsilon}^{pl} : \dot{\varepsilon}^{pl}}\, dt \tag{1}$$

The mesh size of brace member is as the same as gusset plates in all of current FE models. It is worth mentioning that PEEQ which is directly extracted from the FE analysis, is the representative of the plastic equivalent strain. With regard to the experimental results reported by Yoo (2006), and by considering the frame drift ratios corresponding to crack initiation cycles of the brace middle length and gusset plates, the critical value of PEEQ is considered equal to 2.4 for brace, and equal to 1.47 for gusset plate. It should be mentioned that, the plastic equivalent strain is greater at the outer surface than the inner surface of corners/web of the mid-length plastic hinge of the verification brace. This result is totally in consistent with the results evaluated by Haddad (2015).

In order to analyze the failure mechanisms of BSCBFs, ductility capacities (μ_c) of the models have been investigated (Eq. (2)).

$$\mu_c = \Delta_c / \Delta_y \tag{2}$$

Δ_c represents the ultimate displacement of the systems corresponding to the failure cycle, and Δ_y is the displacement of the systems corresponding to the brace yielding. The ductility capacity of the verified model has been found to be 3.2.

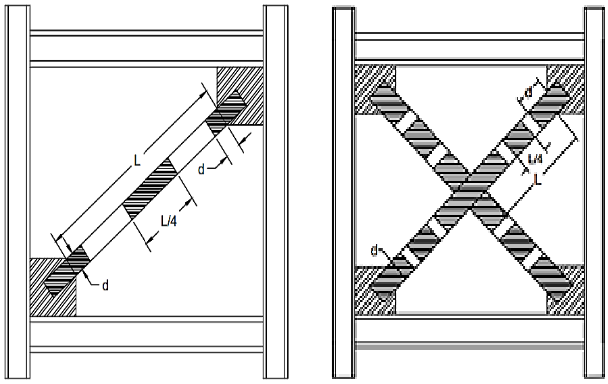

Fig. 6 Protected zones of single diagonal and X-braced BSCBFs (blacked zones) (AISC 2010a and 2016)

3. Current criteria for seismic design of BSCBFs

In order to design BSCBFs based on AISC-341 provision, braced frames are intended to provide significant inelastic deformation capacity through brace buckling as well as tension yielding. Therefore, limitations of width-to-thickness ratio (*b*/*t*) and overall *KL*/*r* slenderness ratio are to be satisfied as follows:

(1) $b/t \le 0.3\sqrt{E/F_y}$, for compression members built up of angle or channel sections.
(2) $KL/r \le 200$, for all SCBFs.

For single diagonal braces in BSCBFs, brace members should comply with following requirements:

(1) The spacing of stitches in built-up braces must be uniform.
(2) Slenderness ratio of individual elements between the stitches (a/r_i) should not exceed 0.4 times the governing slenderness ratio of the built-up member.
(3) Stitch connectors should not be located within the middle one-fourth of the clear brace length and a zone adjacent to each connection equal to the brace depth in the plane of buckling (Protected zones of built up braces) (Fig. 6).

For X-braced models, the protected zone of the braces is shown in Fig. 6 too.

The seismic requirements mentioned above have not changed in AISC 341-16, except the first one, which include R_y value (the ratio of expected yield stress to specified minimum yield stress F_y) on the limitation of width-to-thickness ratio of highly ductile compression members. Therefore, braces should satisfy the limitation of $b/t \le 0.32\sqrt{E/R_yF_y}$ (AISC 2016).

4. Evaluation of seismic criteria of BSCBFs

In order to evaluate current BSCBF seismic criteria, some different FE models are developed to examine seismic requirements. The frame of models are set equal to the verification model except the brace section profiles. As it is observed in Table 2 and Fig. 7, different types of built-up members such as double angle and double channel braces have been employed in both types of single diagonal and X-braced frames. In such braces, stitch connector distance plays a significant role in the failure procedures of BSCBFs. In order to achieve desirable results, it has been tried to set the stitches in various locations among the built-up braces and figure out the seismic criteria like slenderness ratio $((L_i/r_i)/(L/r)_{\max})$ and protected zones.

4.1 Description of the models

According to the Table 2, models are all categorized in highly ductile members because all sections are satisfying width-to-thickness ratios for highly ductile compression members (AISC 2016). The first two letters of the models show type and size of the section forming the brace. For example, C5 represents a section composed of double channel braces (i.e., AISC profile shape of C5×9, Fig. 7 represents the dimensions in centimeters), L3 is the section composed of double angle braces (i.e., AISC profile shape of L3×3×1/2, Fig. 7 represents the dimensions in centimeters); the next letter F or B represents face-to-face or back-to-back connection types. The S or SS represents lateral stitches (parallel to the flanges) or vertical stitches (parallel to the webs). The number after S or SS shows the number of stitch connectors along the built-up braces. 2 t and 6 t represent linear and elliptical clearances in gusset plates (i.e., twice and six times of gusset plate thickness). The ratio of individual slenderness ratio of elements between the stitch connectors to the governing slenderness ratio (i.e., $(L_i/r_i)/(L/r)_{\max}$) has been attached at the end of the model designations to describe the models better. The $(L_i/r_i)/(L/r)_{\max}$ ratio in these models varies mainly from 0.4- to 0.75 ratios. In addition, *L*/4 at the end of the model's name shows that the distance between stitches is as the same as the middle protected zone distance of BSCBFs (i.e., a quarter of free brace length) (Fig. 6).

All of FE models satisfy the modified effective slenderness ratio of the built-up brace members (i.e., $(KL/r)_m \le 200$). In this regard, Eq. (3) demonstrates the calculation for the modified effective slenderness ratio of these members (AISC 2010b).

$$\begin{aligned} L_i/r_i \le 40 &\rightarrow (KL/r)_m = (KL/r)_0 \\ L_i/r_i > 40 &\rightarrow (KL/r)_m = \sqrt{(KL/r)_0^2 + (k_iL_i/r_i)^2} \end{aligned} \tag{3}$$

In Eq. (3), $(KL/r)_m$ and $(KL/r)_0$ show the modified and unmodified effective slenderness ratios of built-up braces, L_i shows the distance between stitches; r_i and r represent the minimum gyration radius of an individual and total built-up sections. L is the brace free length of diagonal frames (Fig. 6), and k_i is a constant that depends on section types of the built-up braces. For the face-to-face double channels, k_i should be equal to 0.86, and for back-to-back double channels, it should be equal to 0.75. Additionally, k_i for the face-to-face and back-to-back double angles should be set equal to 0.86 and 0.5 (AISC 2010b). Hawileh *et al.* (2012) have experimentally studied ultimate axial capacity of side-to-side steel built-up members with different

Table 2 Description of the seismic models (single diagonal-braced frames)

Model designation	Connector dimension (cm)	Connector distances (L_i) (cm)	Governing slenderness ratio (L/r)	Individual slenderness ratio between two connectors (L_i/r_i)	Slenderness ratio $(L_i/r_i)/(L/r)_{max}$	End brace clearance in gussets	Section geometry
			Diagonal double channel braces				
			Face-to-face connection				
C5FS4-6t-0.4	8.8*4.4*0.7	38.0	75.1	30.7	0.40	6t	
C5FS4-6t-0.45	8.8*4.4*0.7	42.0	75.1	34.0	0.45	6t	
C5FS4-6t-0.5	8.8*4.4*0.7	47.0	75.1	38.0	0.50	6t	
C5FS4-6t-0.55	8.8*4.4*0.7	58.0	85.3	46.9	0.55	6t	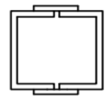
C5FS4-6t-0.6	8.8*4.4*0.7	63.0	87.0	51.0	0.60	6t	
C5FS4-6t-0.65	8.8*4.4*0.7	71.0	89.9	57.5	0.65	6t	
C5FS4-6t-0.7-L/4	8.8*4.4*0.7	81.1	94.0	65.7	0.70	6t	
C5FS4-6t-0.75	8.8*4.4*0.7	85.5	95.5	69.3	0.75	6t	
			Back-to-back connection				
C5BS4-6t-0.4	8.8*4.4*0.7	48.0	96.0	38.8	0.40	6t	
C5BS4-6t-0.45	8.8*4.4*0.7	57.0	102.0	46.1	0.45	6t	
C5BS4-6t-0.5	8.8*4.4*0.7	65.0	103.8	52.6	0.50	6t	
C5BS4-6t-0.55	8.8*4.4*0.7	72.0	105.5	58.3	0.55	6t	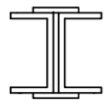
C5BS4-6t-0.6	8.8*4.4*0.7	79.0	107.3	64.0	0.60	6t	
C5BS4-6t-0.61-L/4	8.8*4.4*0.7	81.1	107.9	65.7	0.61	6t	
C5BS4-6t-0.65	8.8*4.4*0.7	88.0	109.9	71.2	0.65	6t	
			Diagonal double angle braces				
			Back-to-back connection				
L3BS2-2t-0.45	14.5*4.4*0.8	47.0	70.5	31.7	0.45	2t	
L3BS2-2t-0.6-L/4	14.5*4.4*0.8	66.4	74.0	44.8	0.60	2t	
L3BS2-2t-0.65	14.5*4.4*0.8	72.0	74.5	48.6	0.65	2t	
L3BS2-2t-0.7	14.5*4.4*0.8	78.0	75.2	52.7	0.70	2t	
L3BS2-2t-0.75	14.5*4.4*0.8	85.0	76.1	57.4	0.75	2t	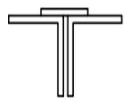
L3BS4-6t-0.4	14.5*4.4*0.8	50.0	86.1	33.7	0.40	6t	
L3BS4-6t-0.55	14.5*4.4*0.8	71.0	89.3	48.0	0.55	6t	
L3BS4-6t-0.6-L/4	14.5*4.4*0.8	81.1	90.3	54.8	0.60	6t	
L3BS4-6t-0.75	14.5*4.4*0.8	99.0	92.3	66.9	0.73	6t	
			X-braced double channel braces				
			Face-to-face connection				
C5FS2-0.4	8.8*4.4*0.7	18.0	40.8	14.5	0.36	6t	
C5FS2-0.55	8.8*4.4*0.7	26.0	40.8	21.0	0.52	6t	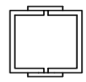
C5FS2-0.6	8.8*4.4*0.7	30.0	40.8	24.3	0.60	6t	
C5FS2-0.75-L/4	8.8*4.4*0.7	36.9	40.8	29.9	0.73	6t	
			Back-to-back connection				
C5BS2-0.4	8.8*4.4*0.7	28.0	57.5	22.6	0.40	6t	
C5BS2-0.55-L/4	8.8*4.4*0.7	36.9	57.5	29.9	0.52	6t	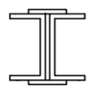
C5BS2-0.65	8.8*4.4*0.7	45.0	57.5	36.4	0.63	6t	
C5BS2-0.75	8.8*4.4*0.7	63.0	69.1	51.0	0.74	6t	
			X-braced double angle braces				
			Face-to-face connection				
L3FSS4-0.4	14.5*4.4*1.7	20.0	40.3	13.5	0.34	6t	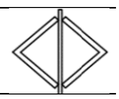
L3FSS2-0.65-L/4	14.5*4.4*1.7	36.8	40.3	24.8	0.62	6t	
			Back-to-back connection				
L3BS4-0.4	14.5*4.4*1	20.0	37.3	13.5	0.36	6t	
L3BS2-0.4	14.5*4.4*1	20.0	37.3	13.5	0.36	6t	
L3BS2-0.6	14.5*4.4*1	31.0	37.3	20.9	0.56	6t	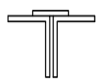
L3BS2-0.7-L/4	14.5*4.4*1	36.8	37.3	24.8	0.66	6t	
L3BS2-0.75	14.5*4.4*1	40.0	37.3	27.0	0.73	6t	

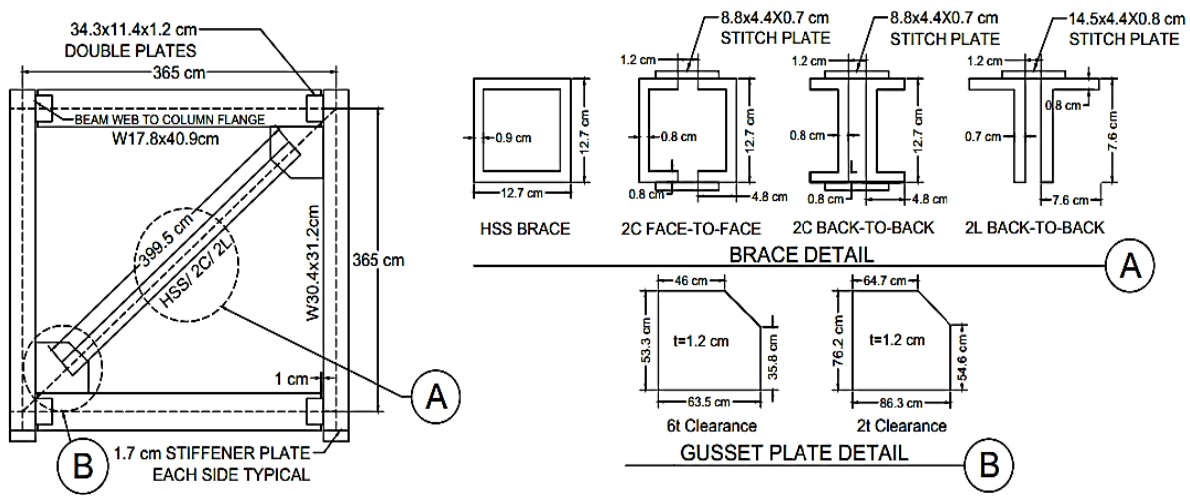

(a) Single diagonal-braced frames

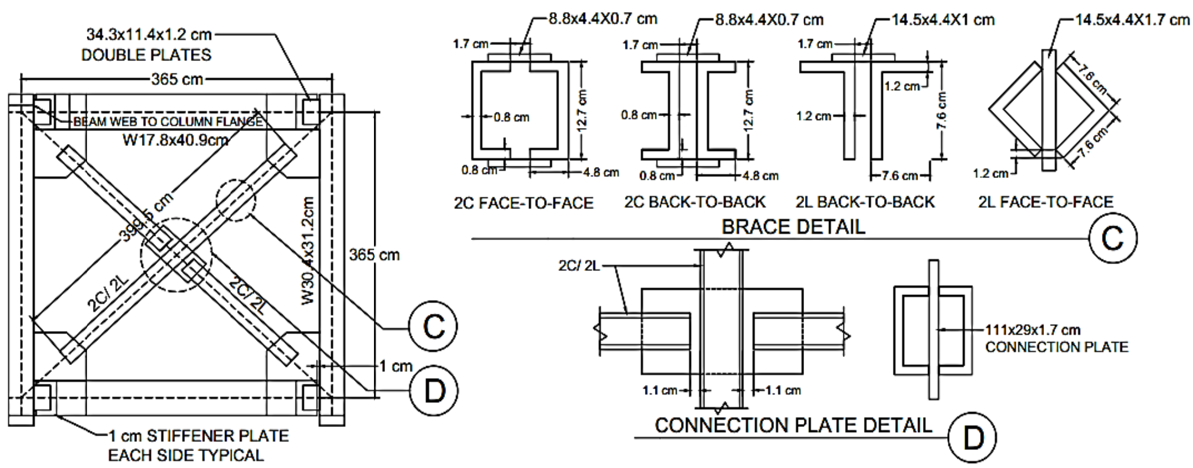

(b) X-braced frames

Fig. 7 Dimensions of the numerically tested frames

slenderness ratios. Their results show that AISC design provisions related to the buckling capacity of such built-up steel compression members are relatively conservative. In order to facilitate the out of plane buckling of the braces as well as the formation of plastic hinges in gusset plates, employing linear or elliptical clearance in gussets is of great importance. In this case, for the free length of diagonal braces, K can be set equal to 1.

Studying on the slenderness of the diagonal members of concentrically X braced steel frames, Metelli (2013) has shown that the effective length of compression member depends on the boundary condition offered by end connections. Corner gusset plates of all X-braced FE models satisfy elliptical clearance distances of 6t, thereby it is appropriate to set the slenderness ratio equal to 1.0 (i.e., K = 1, pinned end conditions) for half diagonal built-up braces.

It is noteworthy that central gusset plate in the face-to-face double channel X-braced frames has been designed based on AISC (2010b). The size of this central gusset plate is about 111×29×1.7 cm. To establish a decent comparison between models, the central gusset plate is not changed in the face-to-face and back-to-back X-braced BSCBFs.

4.2 Results of the single diagonal braces

4.2.1 Double channel face-to-face BSCBFs

According to the results, neither the model satisfying slenderness ratio limitation (i.e., the model of C5FS4-6t-0.4 that observes the 0.4 ratio, $(L_i/r_i)/(L/r)_{\max} \le 0.4$) nor the model obeying the criterion of the protected zone (i.e., C5FS4-6t-0.7-L/4 model) demonstrate desirable cyclic and failure performances. It is due to the results elaborated in Table 3 and depicted in Fig. 9(a). The model indicating the highest compressive and failure resistances in last cycle is the model in which the $(L_i/r_i)/(L/r)_{\max}$ ratio is equal to 0.55 (i.e., C5FS4-6t-0.55 model) rather than 0.4.

This result originated from the possibility of two-fold plastic hinge formations along the braces. FE analysis shows that this phenomenon is most likely to occur in built-up braces in general and in double channel face-to-face diagonal braces in particular (Figs. 10(b) and (c)). In addition, the ductility capacity of the model in which the $(L_i/r_i)/(L/r)_{\max}$ ratio is about 0.55 is higher than the ones satisfying the current seismic criteria.

FE analysis of these braces shows that changing the failure location from stitch weld tearing to the brace failure

Table 3 Results of the seismic models (single diagonal-braced frames)

Model designation	Initial stiffness (kgf/cm)	Last compressive cycle strength (kgf)	Last tensile cycle strength (kgf)	Compressive strength (kgf)	Tensile strength (kgf)	Ductility capacity (μ_c)	Failure location
Diagonal double channel braces							
Face-to-face connection							
C5FS4-6t-0.4	5842.9	55941.6	127566.4	41196.5	113555.5	1.5	SW
C5FS4-6t-0.45	5700.2	56482.0	125251.7	46978.3	109650.0	1.8	SW
C5FS4-6t-0.5	5822.5	56798.1	126006.3	45285.5	116064.0	1.9	SW
C5FS4-6t-0.55	5791.9	59439.2	119663.6	49925.3	113127.3	1.9	SW
C5FS4-6t-0.6	5781.7	56318.9	134174.2	47161.8	143474.0	2.9	MB
C5FS4-6t-0.65	5710.4	55727.4	128066.1	48252.9	117144.9	1.9	SW
C5FS4-6t-0.7-L/4	5761.3	56696.2	128637.2	42430.3	112811.2	1.5	SW
C5FS4-6t-0.75	5791.9	55941.6	129351.0	41155.7	114779.2	1.4	SW
Back-to-back connection							
C5BS4-6t-0.4	5904.1	55533.7	127005.6	54269.2	125363.9	3.3	MB
C5BS4-6t-0.45	5853.1	55849.8	126781.3	55849.8	125863.5	3.2	MB-GW
C5BS4-6t-0.5	5853.1	55870.2	127158.6	55870.2	127158.6	3.3	GW-MB
C5BS4-6t-0.55	5863.3	55747.8	124945.8	55747.8	124945.8	3.5	GW
C5BS4-6t-0.6	5842.9	55717.2	126230.6	55717.2	126230.6	3.3	GW
C5BS4-6t-0.61-L/4	5873.5	55758.0	126924.0	55635.7	126924.0	3.3	GW
C5BS4-6t-0.65	5842.9	55931.4	126200.0	55788.6	126200.0	3.4	GW
Diagonal double angle braces							
Back-to-back connection							
L3BS2-2t-0.45	6770.9	61866.1	128025.3	53667.6	124996.8	1.8	MB
L3BS2-2t-0.6-L/4	6556.7	61019.8	129595.7	56828.7	128219.1	2.1	MB
L3BS2-2t-0.65	6495.5	60989.2	129412.1	56787.9	128494.4	2.0	MB
L3BS2-2t-0.7	6699.5	60662.9	128688.1	56431.0	128004.9	2.1	MB
L3BS2-2t-0.75	6444.6	62610.5	131563.7	55798.8	149500.5	1.3	MB
L3BS4-6t-0.4	5771.5	58205.4	124364.5	49792.7	143300.7	2.8	MB
L3BS4-6t-0.55	5791.9	58093.2	124395.1	49874.3	143820.7	2.7	MB
L3BS4-6t-0.6-L/4	5924.5	58368.5	126006.3	53382.1	138742.5	3.2	MB
L3BS4-6t-0.75	5863.3	57807.7	126322.4	56787.9	124874.4	3.0	MB

mechanism is desirable to provide the highest ductility capacity (i.e., C5FS4-6t-0.6 model). Taking this into account, the protected zone can be shorten to one-fifth of the built-up member length rather than its one-fourth length (Fig. 8(a)).

FE results show that local buckling prognostication of these types of braces is difficult. Hence, the PEEQ curves, based on their development and critical value achievement, should be compared in an appropriate manner. PEEQ curves of these braces are compared in two separate divisions due to the same failure location of each assortment (Figs. 11(a) and (b)).

As shown in Fig. 11(a), it is clear that the growth of plastic equivalent strain in the model obeying the $(L_i\ /\ r_i)$/

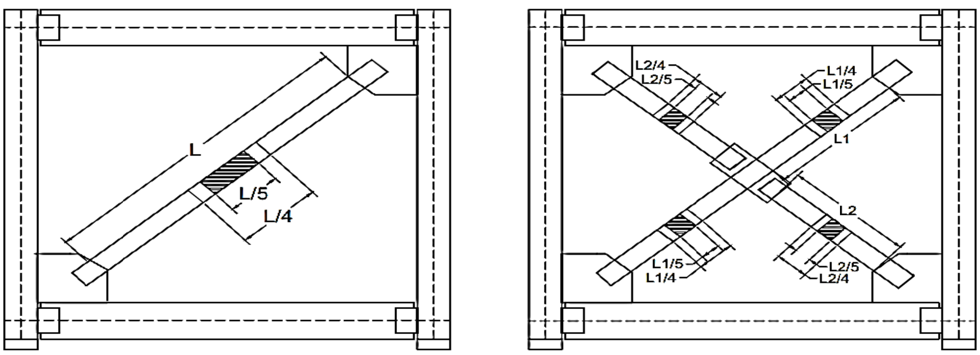

(a) Single diagonal braces (b) X-braced frames

Fig. 8 Proposed middle protected zones for BSCBFs (blacked zones)

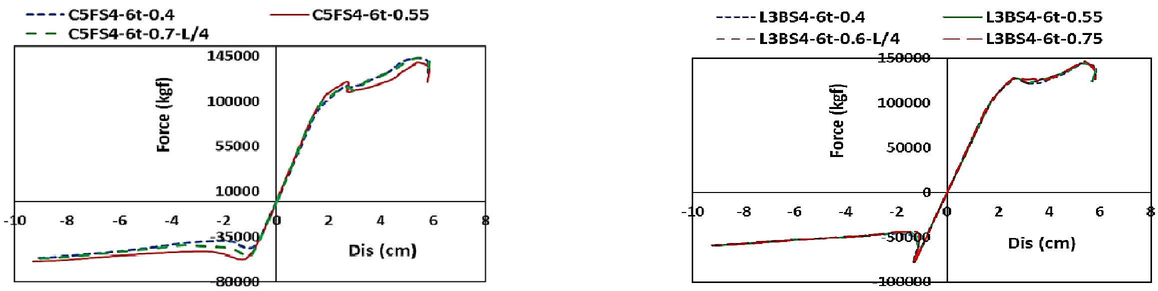

(a) Diagonal double channel face-to-face BSCBFs (b) Diagonal double angle back-to-back BSCBFs

Fig. 9 Force-displacement curve envelop of cyclic results

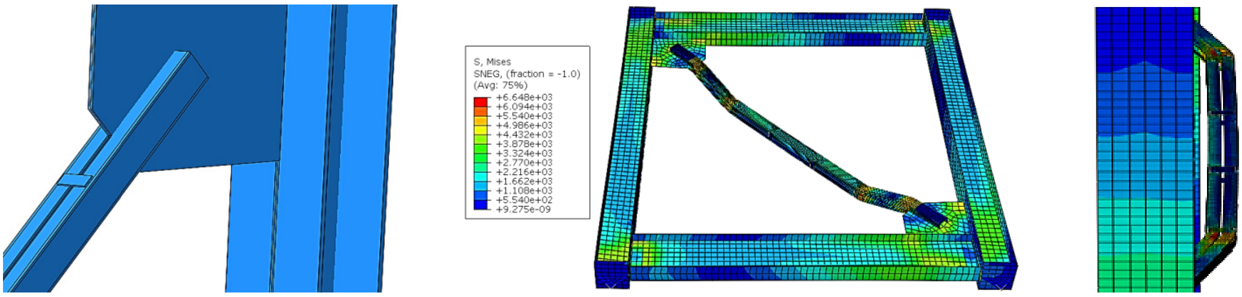

(a) Diagonal double channel face-to-face models (b) C5FS4-6t-0.55 model (c) C5FS4-6t-0.55 model

Fig. 10 BSCBF configurations, Von Mises Stress distributions, and the brace local buckling of seismic models

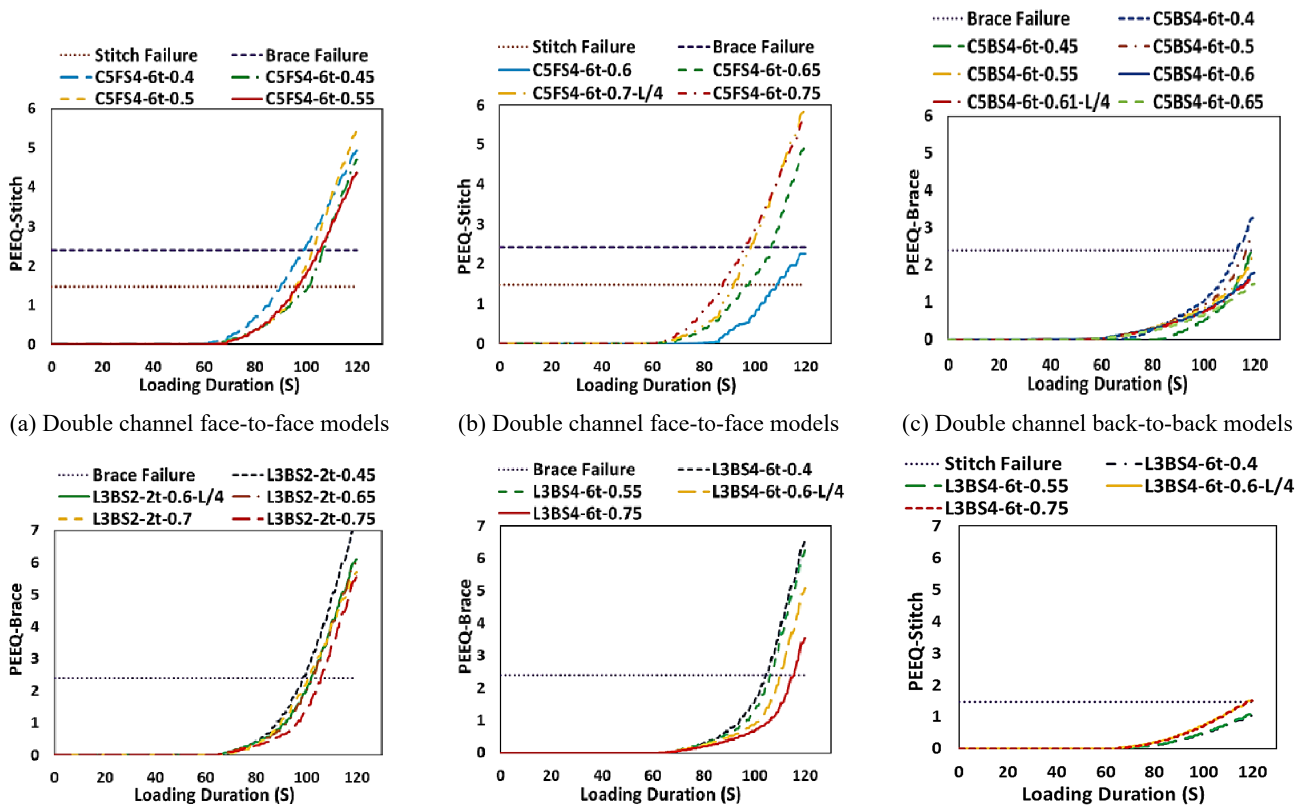

(a) Double channel face-to-face models (b) Double channel face-to-face models (c) Double channel back-to-back models

(d) Double angle back-to-back models (e) Double angle back-to-back models (f) Double angle back-to-back models

Fig. 11 Failure results of single diagonal BSCBFs (plastic equivalent strain curves)

$(L/r)_{\max} \leq 0.4$ ratio happens much earlier and is more critical than the suggested model which has the $(L_i/r_i)/(L/r)_{\max} \leq 0.55$ limitation. Also, the ultimate value of PEEQ for C5FS4-6t-0.55 model is equal to 4.3 and lower than all other comparison models. This parameter has been obtained equal to 4.9 for C5FS4-6t-0.4 model. In addition, based on Fig. 11(b), plastic equivalent strain growth in the models satisfying the limitation of the protected zone (i.e., the middle one-fourth length) is more critical than the model proposes one-fifth ratio for the protected zone (i.e., C5FS4-6t-0.6 model).

Moreover, ductility capacity of the model that suggests one-fifth ratio for the middle protected zone length (i.e., C5FS4-6t-0.6) is the highest one compared to the other related models (Fig. 12(a)).

In conclusion, among what has mentioned for the cyclic and failure behavior of double channel face-to-face models, the current seismic procedures of AISC-341 seem conservative. Thus, the $(L_i/r_i)/(L/r)_{\max} \leq 0.55$ limitation can be suggested for developing the cyclic behavior of such systems. Additionally, a middle protected zone equal to one-fifth length of the brace will be proposed to develop the failure behaviors such as compressive strength as well as the ductility capacity. In the result tables (Tables 3-4), MB shows the failure location at mid brace, and B shows the brace failure. Moreover, SW represents stitch weld, and GW is the gusset weld failure.

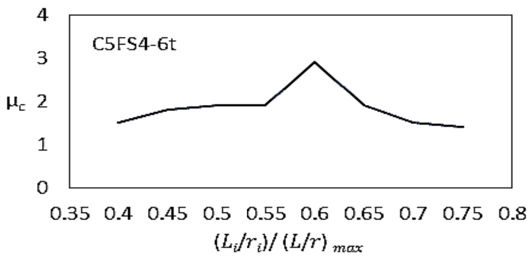

(a) C5FS4-6t diagonal braces

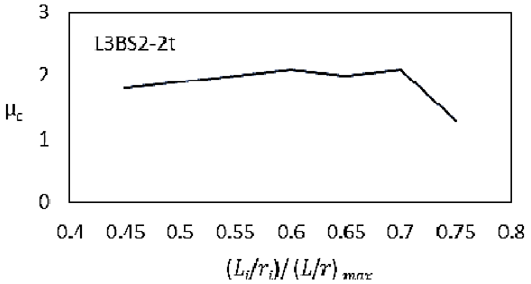

(b) L3BS2-2t diagonal braces

Fig. 12 Ductility capacity ratios

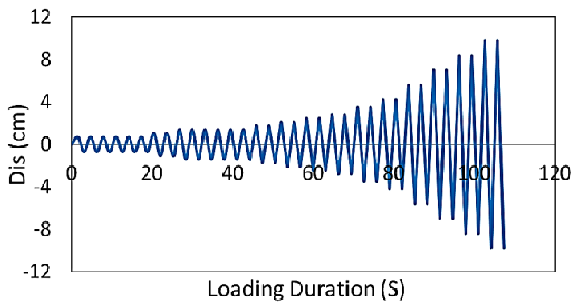

Fig. 13 Cyclic loading based on ATC-24 (1992)

4.2.2 Double channel back-to-back BSCBFs

Results of double channel back-to-back BCBFs illustrate that increasing the $(L_i/r_i)/(L/r)_{\max}$ ratio in the range of 0.4- to 0.65 does not really modify the last compressive cycle resistance. This process can slightly increase the compressive strength and the ductility capacity of such models. In addition, increasing the ratio can change the failure location from the middle brace to the gusset welds. Based on the Fig. 11(c), brace PEEQ curves show that the larger stitch distances the built-up brace has, the later the brace gets its critical value. Thus, in order to make the crack initiations of the brace delayed, the $(L_i/r_i)/(L/r)_{\max}$ ratio should be increased. By doing so, it does not need to change the middle protected zone of these braces; and the current protected zone seem to be a decent length for back-to-back models.

4.2.3 Double angle back-to-back BSCBFs

In this section, two types of diagonal back-to-back double angle BSCBFs containing different gusset plates and number of stitches have been analyzed. The results are shown in the Fig. 9(b) and Figs. 11(d), (e) and (f).

Results in both back-to-back double angle categories show that increasing the $(L_i/r_i)/(L/r)_{\max}$ ratio does not really change the cyclic behavior of these systems (Fig. 9(b)). On the other hand, compressive strength of these models is developing in the light of this increment. Furthermore, brace PEEQ curves imply the fact that the more value the $(L_i/r_i)/(L/r)_{\max}$ slenderness ratio has, the later the curve reaches its critical value, and as the result, the lower the curve has its ultimate value of brace PEEQ, as shown in the Figs. 11(d) and (e). In contrast, by increasing the $(L_i/r_i)/(L/r)_{\max}$ ratio in these types of braces, the stitch PEEQ curves will increase (Fig. 11(f)). Considering the predominant failure of these systems that has to do with the brace failures, the last result can be ignored. Besides these results, the ductility capacity ratios depicted in Fig. 12(b) shows an additional failure evaluation of such BSCBF systems.

In conclusion, the seismic criterion related to the limitation of slenderness ratio of individual members between stitches (i.e., $(L_i/r_i)/(L/r)_{\max} \leq 0.4$), seems to be more conservative for these members; so, in order to modify the failure behavior of such systems, the $(L_i/r_i)/(L/r)_{\max}$ ratio should be increased, even to the ratio of 0.7. In this regard, the middle protected zone of these braces seems reasonable. It is worth mentioning that, cyclic and failure results of back-to-back double angle diagonal BSCBFs are very similar to those of double channel diagonal BSCBFs mentioned earlier. Considering this, results of back-to-back section braces illustrate that the location of failures in these types of braces are mostly in the braces or the gusset plate corners rather than their stitch welds.

4.3 Results of the X-braced frames

X-braced models are subjected to a cyclic inelastic deformation history according to ATC-24 (1992) (Fig. 13).

Fig. 14 shows all X-braced BSCBF models and their specific local buckling. Disconnected braces do not join

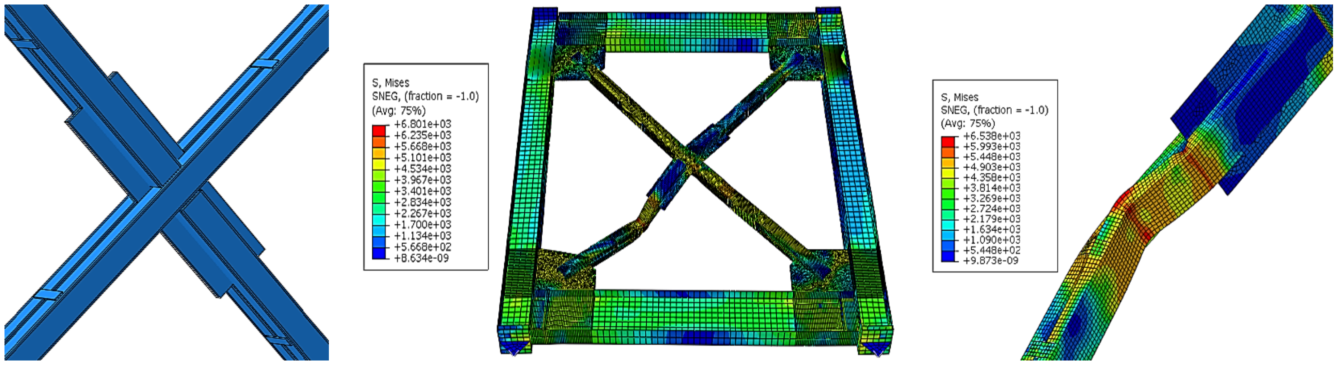

(a) Double channel face-to-face models (C5FS2-0.75-L/4)

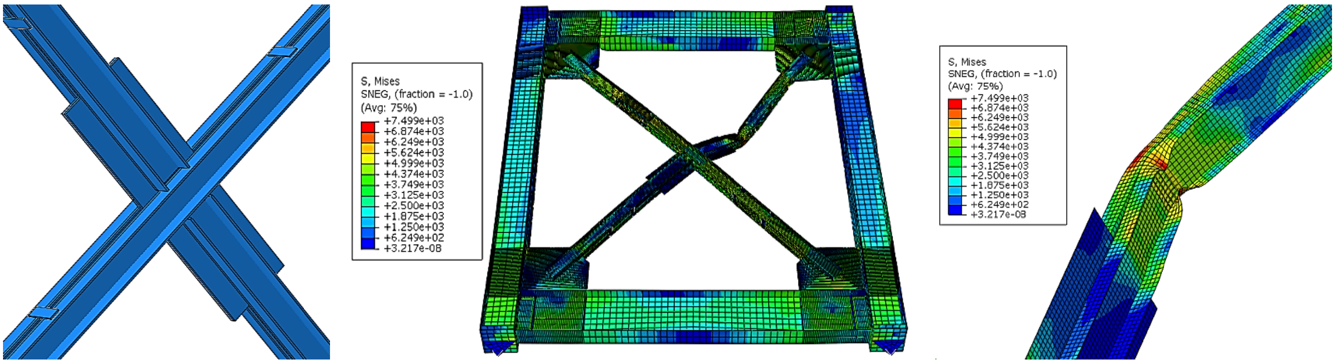

(b) Double channel back-to-back models (C5BS2-0.55-L/4)

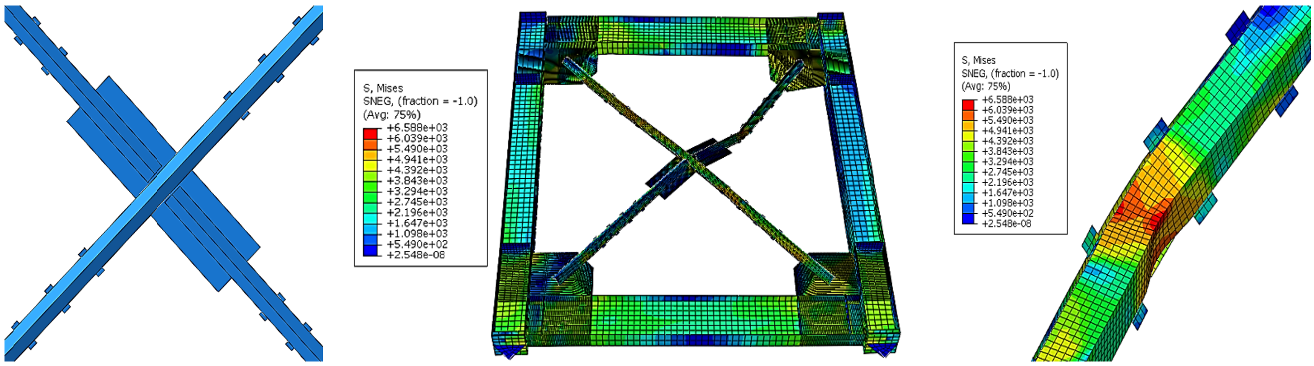

(c) Double angle face-to-face models (L3FSS2-0.65-L/4)

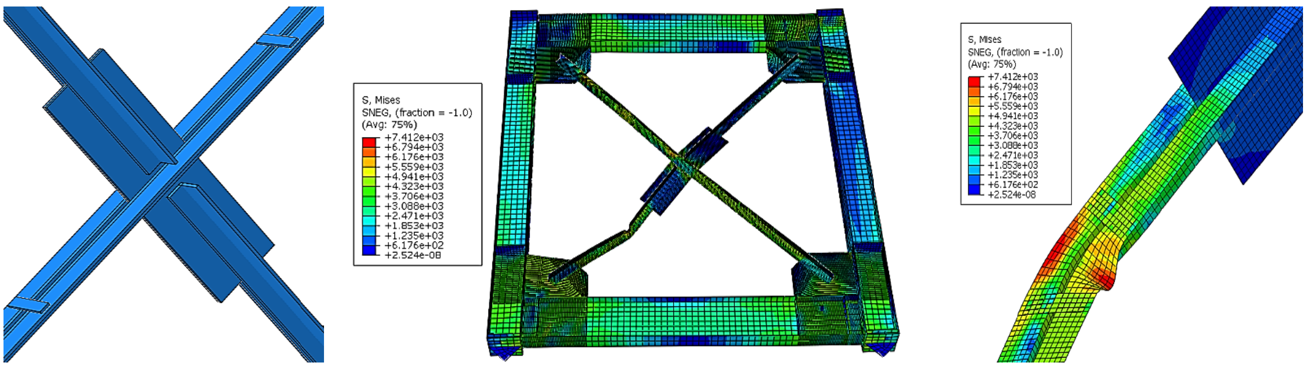

(d) Double angle back-to-back models (L3BS2-0.7-L/4)

Fig. 14 BSCBF configurations, Von Mises Stress distribution, and X-braced local buckling

the continuous member in the center and they completely separate each other in the central gusset plate. Similar to single diagonal BSCBFs, the $(L_i/r_i)/(L/r)_{\max}$ ratio in both compression and tension braces varies from 0.4- to 0.75 ratios. Cyclic and failure results of X-braced BSCBFs have been shown in Table 4 and Figs. 15-17.

Table 4 Results of the seismic models (X-braced frames)

Model designation	Initial stiffness (kgf/cm)	Last compressive cycle strength (kgf)	Last tensile cycle strength (kgf)	Compressive strength (kgf)	Tensile strength (kgf)	Ductility capacity (μ_c)	Failure location
X-braced double channel braces							
Face-to-face connection							
C5FS2-0.4	10625.4	196825.6	204228.7	167386.4	172597.1	3.0	SW
C5FS2-0.55	10574.4	194888.1	204208.3	177869.0	183100.2	3.5	SW
C5FS2-0.6	10574.4	192522.4	209347.7	169527.8	180530.5	3.4	SW-BC
C5FS2-0.75-L/4	10564.2	195785.5	204045.2	186873.1	192828.3	4.7	SW
Back-to-back connection							
C5BS2-0.4	10788.5	186332.7	202515.6	165336.7	171098.1	2.9	B
C5BS2-0.55-L/4	10870.1	182926.8	203025.4	162726.3	171740.6	2.4	B
C5BS2-0.65	10880.3	182223.2	203209.0	167417.0	176553.6	3.2	B
C5BS2-0.75	10849.7	177267.4	200190.6	166295.3	171954.7	3.0	B
X-braced double angle braces							
Face-to-face connection							
L3FSS4-0.4	11410.6	190992.8	215058.1	189881.3	209357.9	6.7	SW-B-GW
L3FSS2-0.65-L/4	11594.1	198712.0	213926.2	200109.1	208919.4	9.7	SW-BM
Back-to-back connection							
L3BS4-0.4	10176.7	192430.6	214344.3	182824.9	197304.8	3.6	B
L3BS2-0.4	10176.7	189106.3	209572.0	181234.1	195765.1	3.7	B
L3BS2-0.6	10829.3	190187.2	211254.6	181968.3	194612.8	3.2	B
L3BS2-0.7-L/4	11084.3	189218.5	211305.5	179510.8	195897.6	3.8	B
L3BS2-0.75	11043.5	188994.2	211713.4	180387.7	196540.1	3.7	B

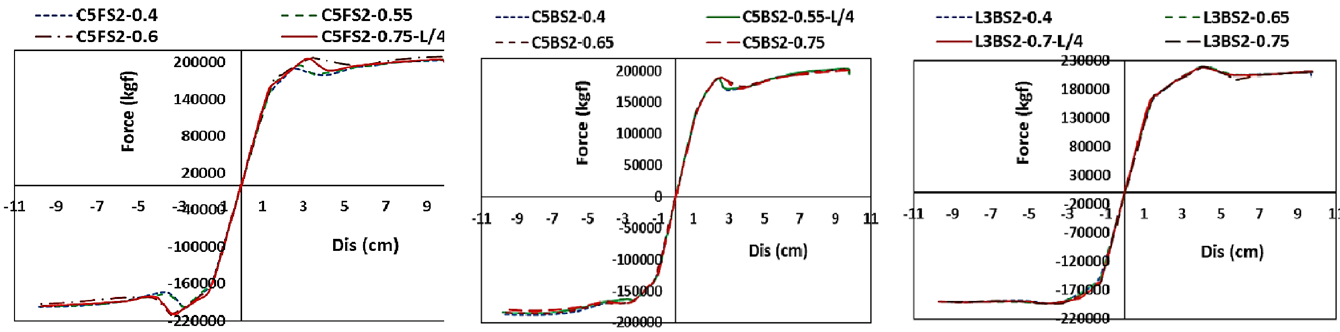

(a) Double channel face-to-face models (b) Double channel back-to-back models (c) Double angle back-to-back models

Fig. 15 Cyclic envelop curves of X-braced models

4.3.1 Double channel face-to-face BSCBFs

Specifically speaking about the double channel face-to-face sections, the results show that the closer the stitches are set in the middle of half-diagonal braces, the lesser value the compressive strength has, and the lesser ductility capacity the model will enjoy (Table 4). Force-displacement envelop curves of these braces have been depicted in Fig. 15(a). It is worth mentioning that in the X-braced built-up frames, the central gusset plates play a significant role to improve the cyclic and failure behaviors. Considering this, stitches along the half braces should be attached in appropriate locations. The FE results show that if the local buckling of the brace locates out of the stitch zones and near the mid gusset plate, the cyclic and failure behavior of the system will be developed. Therefore, based on these results, the protected zones of each compression and tension members (i.e., the middle one-fourth length of a half-diagonal member) should be remained unchanged. This result can increase the $(L_i/r_i)/(L/r)_{\max}$ ratio to the extent of 0.75 for these BSCBFs.

The plastic equivalent strain growth of stitches in Fig. 16(a), and the ductility capacity ratios of such members in Fig. 17(a) confirm the latest result, emphasizing the conservativeness of $(L_i/r_i)/(L/r)_{\max} \leq 0.4$ limitation for such X-braced frames.

4.3.2 Double channel back-to-back BSCBFs

The results of double channel back-to-back X-braced

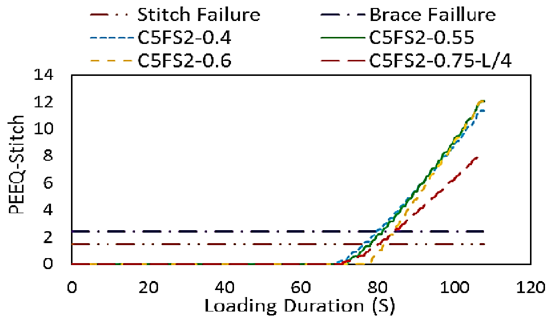

(a) Double channel face-to-face models

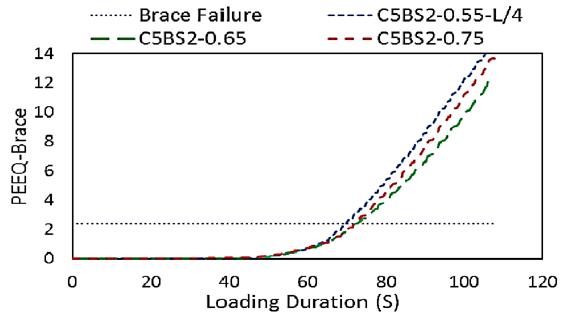

(b) Double channel back-to-back models

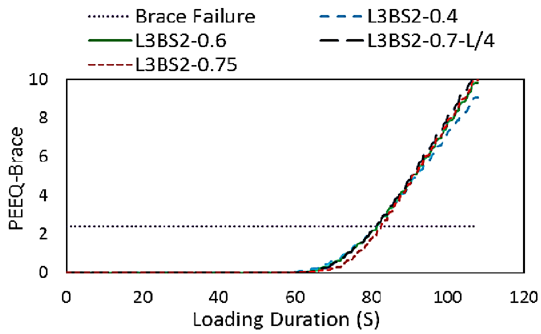

(c) Double angle back-to-back models

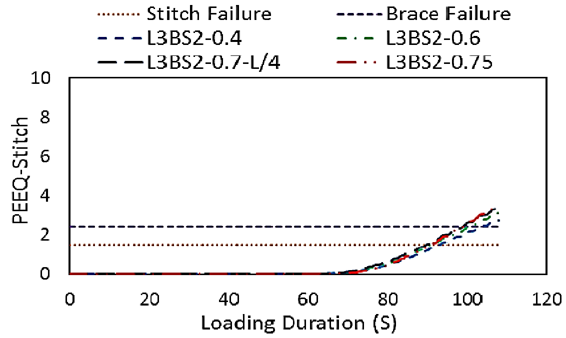

(d) Double angle back-to-back models

Fig. 16 Failure results of X-braced models (plastic equivalent strain curves)

BSCBFs have been provided in Figs. 15(b), 16(b), and 15(b). As far as seismic evaluation of such models is concerned, one of the models satisfying the $(L_i/r_i)/(L/r)_{\max} \leq 0.4$ limitation (i.e., C5BS2-0.4) brings about more desirable cyclic and failure behaviors than other similar models. The buckling location of this model is near the mid gusset plate in both compression and tension members as mentioned earlier for face-to-face connections.

In addition, by increasing the $(L_i/r_i)/(L/r)_{\max}$ ratio from 0.4- to 0.75, the buckling location of half-diagonal braces will be changed and occur in the middle of the braces. Accordingly, the resistant behaviors of such systems will be reduced (Fig. 15(b)). Therefore, in order to modify their cyclic behaviors, the middle protected zone length of each half-diagonal members should be reduced to the one-fifth length of each member (Fig. 8(b)). It is important to say that changing the limitation of $(L_i/r_i)/(L/r)_{\max}$ ratio does not significantly impact on the failure behaviors of such systems, including compressive strength, ductility capacity, and plastic equivalent strain growth (Fig. 16(b)).

Based on the limitations of the $(L_i/r_i)/(L/r)_{\max}$ ratio shown in the Fig. 17(b), ductility capacity of such braces does not significantly change with increasing that ratio.

4.3.3 Double angle back-to-back BSCBFs

Seismic evaluation results of double angle back-to-back sections in X-braced BSCBFs show that variation of protected zones of such braces that results in the changes of $(L_i/r_i)/(L/r)_{\max}$ ratio does not significantly influence on the total cyclic and failure behaviors of these systems as shown in Figs. 15(c) and 16(c). Results related to the growth of stitch PEEQ curves show that the more the $(L_i/r_i)/(L/r)_{\max}$ ratio has been increased along the half braces, the earlier the curves get their critical values (Fig. 16(d)).

5. Built-up brace configuration effects

In this part, cyclic and failure effects of different section

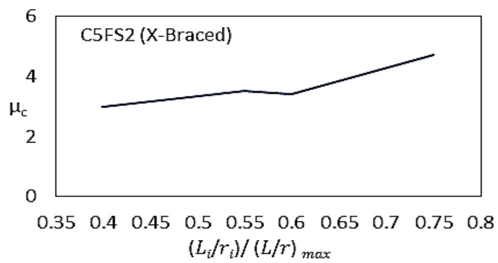

(a) Double channel face-to-face models

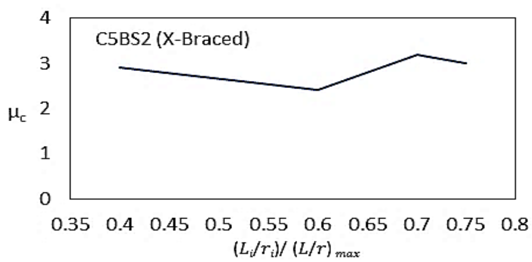

(b) Double channel back-to-back models

Fig. 17 Ductility capacity ratios of X-braced models

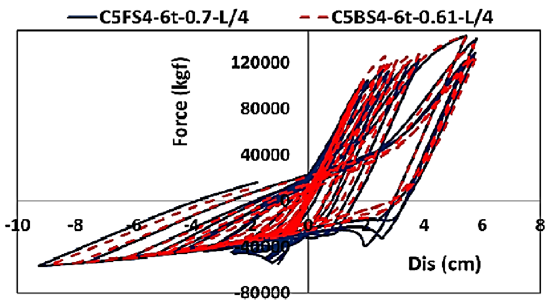

(a) Single diagonal double channel braces

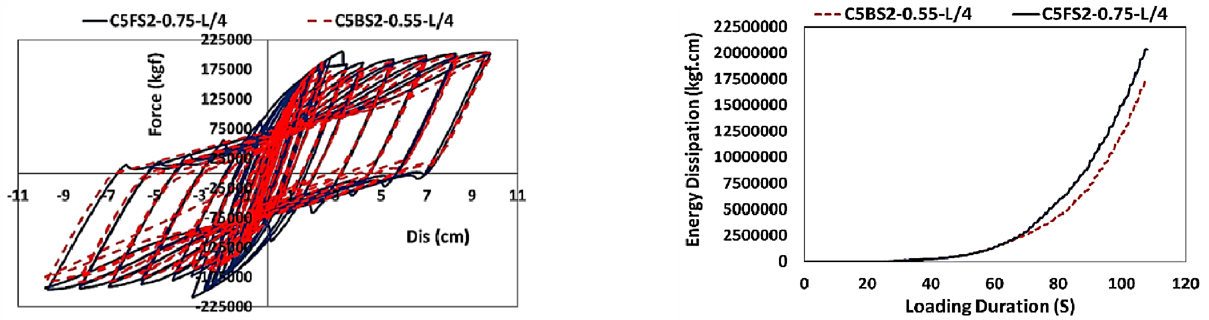

(b) Double channel face-to-face and back-to-back X-braced models

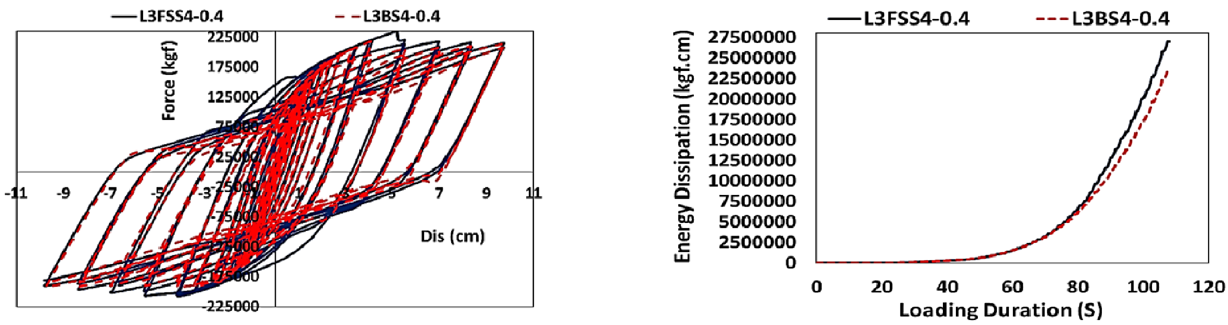

(c) Double angle face-to-face and back-to-back X-braced models

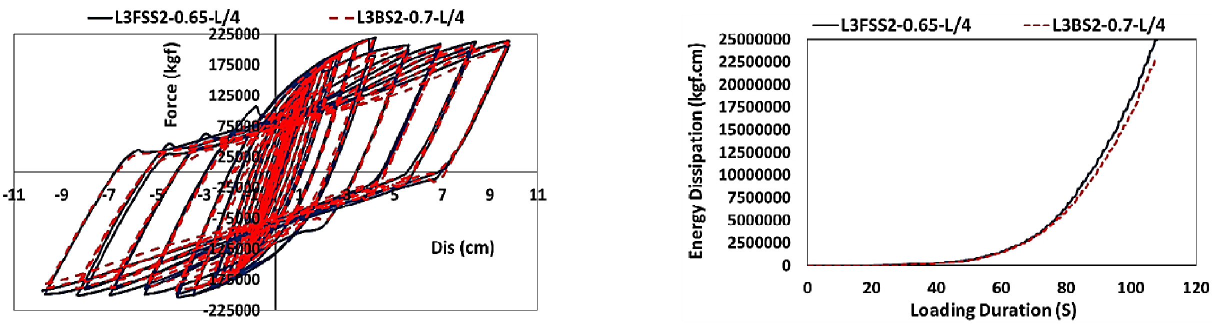

(d) Double angle face-to-face and back-to-back X-braced models

Fig. 18 Built-up brace configuration effects on cyclic behavior and energy dissipation

configurations such as face-to-face and back-to-back sections have been evaluated for the BSCBF models. The comparisons of force-displacement cyclic curves, energy dissipated, and plastic equivalent strain curves of similar face-to-face and back-to-back brace sections are presented in Figs. 18-19. It is of great importance to mention that the compared models are similar to each other in every details such as dimensions, stitch numbers, and distances between stitch connectors. They just have a difference related to their brace connection types (i.e., face-to-face and back-to-back configurations). In order to evaluate the built-up brace configuration effects on ductility capacities of models, comparison results for similar models have been presented graphically in Fig. 19(f).

Based on the cyclic behaviors, plastic equivalent strain growths, and ductility capacities of these BSCBFs, it is clear that cyclic and failure results of all types of X-braced face-to-face models turn out to be better than those of

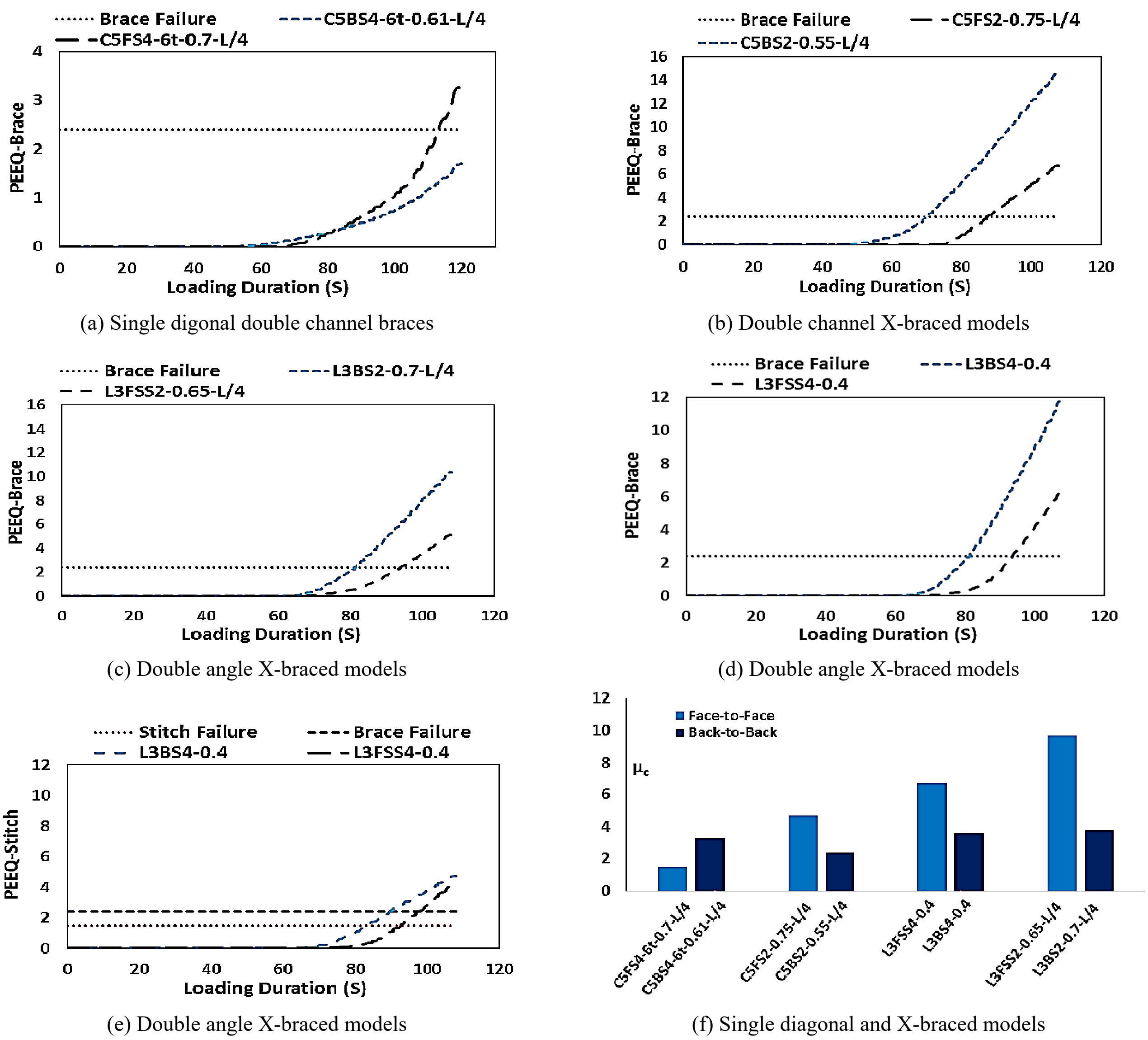

Fig. 19 Built-up brace configuration effects on plastic equivalent strain curves and ductility capacity

similar back-to-back braces.

Furthermore, cyclic evaluation results confirm the importance of frame and gusset plates resistances during the last cycle loadings. This issue is due to the fact of overlapped cyclic curves during the last cycles (Fig. 18).

6. Conclusions

The results reveal that the current criteria of AISC 341 provision are partly conservative; especially, with regard to the limitation of the individual brace slenderness ratio between stitches, which must be less than 0.4 times of the overall slenderness ratio of the built-up braces, and stitch locations that must satisfy BSCBF protected zones. It appears that the seismic criteria for different types of built-up sections, namely double channel and double angle sections should be different. This is due to the different seismic behaviors of all types of BSCBFs as they undergo cyclic deformations.

The failure results of single diagonal BSCBFs, regarding both ductility capacity and plastic equivalent strain growth, show that the slenderness limitation of 0.4 ratio could increase. For instance, the slenderness limitation of 0.6 ratio for double channel face-to-face members, 0.65 ratio for double channel back-to-back ones, and 0.7 ratio for double angle back-to-back BSCBFs have been studied and found satisfactory. Furthermore, it appears that the protected zones of such braces in the middle (i.e., one-fourth length of the brace) could be changed. For example, one-fifth of the brace middle length has been proposed for the protected zone of double channel face-to-face braces.

Seismic evaluations of all types of X-braced models show that observing the protected zone limitation of such braces (i.e., one-fourth middle length of half-diagonal members) has advantages over obeying the 0.4 ratio of slenderness limitation. This is due to the importance of the brace local buckling occurring closer to the mid gusset plate rather than closer to the middle length of half-diagonal braces.

This research shows that different built-up brace configurations, such as face-to-face and back-to-back sections, can affect the cyclic and failure behaviors of BSCBFs. For single diagonal BSCBFs, double channel back-to-back braces are preferred in comparison to the face-to-face models, especially due to their failure results. However, diagonal double angle face-to-face braces act much better than the similar back-to-back ones because of experiencing the lower plastic equivalent strains of the brace. FE analysis for X-braced frames reveals the importance of using face-to-face built-up braces instead of the back-to-back ones.

References

AISC (2010a), ANSI/AISC 341-10, Seismic Provisions for Structural Steel Buildings, American Institute of Steel Construction; Chicago, IL, USA.

AISC (2010b), ANSI/AISC 360-10, Specification for Structural Steel Buildings, American Institute of Steel Construction; Chicago, IL, USA.

AISC (2016), ANSI/AISC 341-16, Seismic Provisions for Structural Steel Buildings, American Institute of Steel Construction; Chicago, IL, USA.

Alipour, M. and Aghakouchak, A. (2013), "Numerical analysis of the nonlinear performance of concentrically braced frames under cyclic loading", *Int. J. Steel Struct.*, **13**(3), 401-419.

Aslani, F. and Goel, S.C. (1992), "Stitch spacing and end fixity in seismic-resistant boxed angle braces", *J. Struct. Eng.*, **118**(10), 2872-2889.

Astaneh-Asl, A. (1998), "Seismic behavior and design of gusset plates", Steel TIPS Report.

Astaneh-Asl, A., Goel, S.C. and Hanson, R.D. (1982), "Cyclic behavior of double angle bracing members with end gusset plates", Research Report No. UMEE82R7; Department of Civil Engineering, The University of Michigan, Ann Arbor, MI, USA.

Astaneh-Asl, A., Goel, S.C. and Hanson, R.D. (1985), "Cyclic out-of-plane buckling of double-angle bracing", *J. Struct. Eng.*, **111**(5), 1135-1153.

ATC-24 (1992), Guidelines for Cyclic Seismic Testing of Components of Steel Structures for Buildings, Applied Technology Council.

D'Aniello, M., La Manna Ambrosino, G., Portioli, F. and Landolfo, R. (2013), "Modelling aspects of the seismic response of steel concentric braced frames", *Steel Compos. Struct., Int. J.*, **15**(5), 539-66.

Fell, B.V. (2008), Large-scale Testing and Simulation of Earthquake-induced Ultra-low Cycle Fatigue in Bracing Members Subjected to Cyclic Inelastic Buckling, University of California Davis, CA, USA.

Fell, B.V., Kanvinde, A.M., Deierlein, G.G. and Myers, A.T. (2009), "Experimental investigation of inelastic cyclic buckling and fracture of steel braces", *J. Struct. Eng.*, **135**(1), 19-32.

Haddad, M. (2015), "Concentric tubular steel braces subjected to seismic loading: Finite element modeling", *J. Constr. Steel Res.*, **104**, 155-166.

Haddad, M. (2017), "Cyclic behavior and finite element modeling of wide flange steel bracing members", *Thin-Wall. Struct.*, **111**, 65-79.

Hadianfard, M.A. and Khakzad, A.R. (2016), "Inelastic buckling and post-buckling behavior of gusset plate connections", *Steel Compos. Struct., Int. J.*, **22**(2), 411-427.

Hassan, M.S., Salawdeh, S. and Goggins, J. (2018), "Determination of geometrical imperfection models in finite element analysis of structural steel hollow sections under cyclic axial loading", *J. Constr. Steel Res.*, **141**, 189-203.

Hawileh, R.A., Abed, F., Abu-Obeidah, A.S. and Abdalla, J.A. (2012), "Experimental investigation of inelastic buckling of built-up steel columns", *Steel Compos. Struct., Int. J.*, **13**(3), 295-308.

Hsu, H.L., Juang, J.L. and Chou, C.H. (2011), "Experimental evaluation on the seismic performance of steel knee braced frame structures with energy dissipation mechanism", *Steel Compos. Struct., Int. J.*, **11**(1), 77-91.

Jain, A.K. and Goel, S.C. (1978), "Hysteresis models for steel members subjected to cyclic buckling or cyclic end moments and buckling", User's guide for DRAIN-2D: EL9 and EL10.

Johnson, S.M. (2005), "Improved seismic performance of special concentrically braced frames", Ph.D. Dissertation; University of Washington, Washington, USA.

Kanyilmaz, A. (2017), "Role of compression diagonals in concentrically braced frames in moderate seismicity: A full scale experimental study", *J. Constr. Steel Res.*, **133**, 1-18.

Lai, J.W., Chen, C.H. and Mahin, S.A. (2010), "Experimental and analytical performance of concentrically braced steel frames", *In Structures Congress*, Orlando, FL, United States, May.

Lee, K. and Bruneau, M. (2005), "Energy dissipation of compression members in concentrically braced frames: Review of experimental data", *J. Struct. Eng.*, **131**(4), 552-559.

Lehman, D.E., Roeder, C.W., Herman, D., Johnson, S. and Kotulka, B. (2008), "Improved seismic performance of gusset plate connections", *J. Struct. Eng. (ASCE)*, **134**(6), 890-901.

Metelli, G. (2013), "Theoretical and experimental study on the cyclic behavior of X braced steel frames", *Eng. Struct.*, **46**, 763-773.

Shaback, B. and Brown, T. (2003), "Behavior of square hollow structural steel braces with end connections under reversed cyclic axial loading", *Can. J. Civil Eng.*, **30**(4), 745-753.

Tirca, L. and Chen, L. (2014), "Numerical simulation of inelastic cyclic response of HSS braces upon fracture", *Adv. Steel Constr.*, **10**(4), 442-462.

Tremblay, R. (2002), "Inelastic seismic response of steel bracing members", *J. Constr. Steel Res.*, **58**(5), 665-701.

Yoo, J.H. (2006), "Analytical investigation on the seismic performance of special concentrically braced frames", Ph.D. Dissertation; University of Washington, Washington, USA.

CC